

Chemical abundance analysis of 19 barium stars

G. C. Yang^{1,2,3}, Y. C. Liang², M. Spite⁴, Y. Q. Chen², G. Zhao², B. Zhang^{1,2}, G. Q. Liu^{5,2}, Y. J. Liu², N. Liu⁶, L. C. Deng², F. Spite⁴, V. Hill⁴, C. X. Zhang⁷

¹College of Physics and Information Engineering, Hebei Normal University, Shijiazhuang 050024, China

²Key Laboratory of Optical Astronomy, National Astronomical Observatories, Chinese Academy of Sciences, Beijing 100012, China; ycliang@bao.ac.cn

³Graduate School of the Chinese Academy of Sciences, Beijing 100049, China

⁴GEPI, Observatoire de Paris-Meudon, 92195 Meudon, France

⁵Physics Department and Tsinghua Center for Astrophysics, Tsinghua University, Beijing 100084, China

⁶Astronomy Department, Beijing Normal University, Beijing 100875, China

⁷Department of Physics, Shijiazhuang University, Shijiazhuang 050035, China

Abstract We aim at deriving accurate atmospheric parameters and chemical abundances of 19 barium (Ba) stars, including both strong and mild Ba stars, based on the high signal-to-noise ratio and high resolution Echelle spectra obtained from the 2.16 m telescope at Xinglong station of National Astronomical Observatories, Chinese Academy of Sciences. The chemical abundances of the sample stars were obtained from an LTE, plane-parallel and line-blanketed atmospheric model by inputting the atmospheric parameters (effective temperatures T_{eff} , surface gravities $\log g$, metallicity $[\text{Fe}/\text{H}]$ and microturbulent velocity ξ_t) and equivalent widths of stellar absorption lines. These samples of Ba stars are giants indicated by atmospheric parameters, metallicities and kinematic analysis about UVW velocity. Chemical abundances of 17 elements were obtained for these Ba stars. Their Na, Al, α - and iron-peak elements (O, Na, Mg, Al, Si, Ca, Sc, Ti, V, Cr, Mn, Ni) are similar to the solar abundances. Our samples of Ba stars show obvious overabundances of neutron-capture (n -capture) process elements relative to the Sun. Their median abundances of $[\text{Ba}/\text{Fe}]$, $[\text{La}/\text{Fe}]$ and $[\text{Eu}/\text{Fe}]$ are 0.54, 0.65 and 0.40, respectively. The Y I and Zr I abundances are lower than Ba, La and Eu, but higher than the α - and iron-peak elements for the strong Ba stars and similar to the iron-peak elements for the mild stars. There exists a positive correlation between Ba intensity and $[\text{Ba}/\text{Fe}]$. For the n -capture elements (Y, Zr, Ba, La), there is an anti-correlation between their $[\text{X}/\text{Fe}]$ and $[\text{Fe}/\text{H}]$. We identify nine of our sample stars as strong Ba stars with $[\text{Ba}/\text{Fe}] > 0.6$ where seven of them have Ba intensity $\text{Ba}=2\text{--}5$, one has $\text{Ba}=1.5$ and another one has $\text{Ba}=1.0$. The remaining ten stars are classified as mild Ba stars with $0.17 < [\text{Ba}/\text{Fe}] < 0.54$.

Key words: Methods: observational – stars: abundances – stars: atmospheres – Stars: chemically peculiar – Stars: kinematics and dynamics – Stars: late-type

* Based on spectroscopic observations in National Astronomical Observatory, Chinese Academy of Sciences (NAOC) (Xinglong, China) .

1 INTRODUCTION

Barium (Ba) stars belong to a distinct class of peculiar giants which were first identified by Bidelman & Keenan (1951). The stars of this group are G to K giants, and in their spectra there are abnormally strong lines of *s*-process elements, especially Ba II at 4554 Å, as well as enhanced CH, CN and C₂ molecular bands. Besides Ba and Sr, other heavy elements such as Y, Zr, La, Ce, Pr, Nd and Sm are also enhanced. The general properties of Ba stars were reviewed in detail in McClure (1984), and the chemical composition of Ba stars have been reviewed by Lambert (1985, 1988).

Burbidge et al. (1957) identified the mode of synthesis with slow *n*-capture process (*s*-process) being responsible for the production of the majority of the isotopes heavier than iron. The later works on *s*-process enrichment usually parameterize the amount of ¹³C burnt during the *s*-process operation in the interior of asymptotic giant branch (AGB) stars (Straniero et al. 1995, 1997; Busso et al. 1995, 1999, 2001; Gallino et al. 1998). They suggested that ¹³C was completely burnt in the radiative condition, and the resulting *s*-process nucleosynthesis occurred during the quiescent interpulse period, instead of the convective thermal pulse. ²²Ne(α, n)²⁵Mg was still active for a very short period during the convective pulse and had a minor influence on the whole process of nucleosynthesis. In thermally pulsating AGB stars (TP-AGBs), the deep dredge-up phenomenon that follows the thermal pulses, the so-called third dredge-up, mixes some of the processed material to the atmosphere, where it becomes accessible to observations. The mechanism of *s*-process is relatively clear, whereas the astrophysical site of the rapid *n*-capture process (*r*-process) is debated, although it is believed to take place in supernova explosions of massive stars (Cowan et al. 1991; Sneden et al. 2008).

Because of their low luminosity, low mass and the absence of the unstable nucleus ⁹⁹Tc ($\tau_{1/2} = 2 \times 10^5$ yr), Ba stars are not TP-AGB stars. It is generally believed that they belong to binary systems and that the overabundance of their heavy elements would be caused by the accretion of the matter ejected by their more massive companions (now a white dwarf) in their TP-AGB phase about 1×10^6 years ago (McClure et al. 1980; Han et al. 1995; Jorissen et al. 1998; Liang et al. 2000). They should not have evolved to the TP-AGB stage to synthesize these heavy elements yet.

McClure et al. (1980) revealed that most Ba stars, maybe all of them, show variations in radial-velocity suggesting the presence of companions. The orbital elements of a number of Ba stars in binary systems have been measured (Carquillat et al. 1998; Udry et al. 1998a,b; Jorissen et al. 1998). The determination of the chemical abundances of a large sample of Ba stars must be very important for understanding their formation scenario and the abundance patterns in the ejecta of AGB stars.

It is often difficult to study the chemical abundances of such cold stars with M, S and C spectral types and with strong TiO absorption lines. Lu (1991) presented a table of 389 Ba stars with an estimate of their Ba intensities (from 1 to 5) following Lu et al. (1983) on the scale defined by Warner (1965) and based on the strength of Ba II 4554 Å line. We could roughly divide the Ba stars into two classes: weak (mild) Ba stars (with Ba<2) and strong Ba stars (with Ba=2-5). But we will consider [Ba/Fe] abundance ratios as a stricter diagnostic for strong and mild Ba stars in this work.

Many studies have tried to analyze in detail the abundances of Ba stars based on high resolution and high signal-to-noise (*S/N*) spectra. Začs (1994) analyzed the chemical abundances of a sample of 31 Ba stars and normal G-K giants. Allen & Barbuy (2006a,b) analyzed 26 Ba stars. Smiljanic et al. (2007) analyzed 13 sample stars. In addition, the chemical composition of 5, 16 and 1 Ba stars was studied by Boyarchuk et al. (2002), Antipova et al. (2004) and Yushchenko et al. (2004), respectively. Other available analyses are mostly based on data with lower *S/N* ratio (Pilachowski et al. 1977; Smith 1984; Kovacs 1985; Luck & Bond 1991).

As a consequence, the number of well studied Ba stars is still small compared to the 389 stars listed in Lu (1991). A detailed analysis of the abundances of a large sample of Ba stars is necessary to reveal their properties and formation scenario. Moreover, most of the previous studies have focussed on strong Ba stars. In this work, we aim to extend the sample to many mild Ba stars with a relatively low Ba intensity.

In 2000, we started a project of analyzing the chemical composition of a large sample of Ba stars. In 2000, 2001, 2004 and 2005, high resolution Echelle spectra with high *S/N* ratio were obtained with the

2.16 m telescope located at Xinglong station, China. Liang et al. (2003) and Liu et al. (2009) analyzed four and eight typical Ba stars, respectively. In our present work, we analyze in detail the chemical abundances of the remaining 19 Ba stars.

This paper is organized as follows. In Section 2, we describe the observations and analysis methods. In Section 3, we present the atmospheric parameters of the stars. In Section 4, we define the adopted atmospheric model and discuss the choice of spectral lines. We analyze the element abundances and the uncertainty, and the relation between the Ba intensity and [Ba/Fe] in Section 5. In Section 6, we analyze their UVW kinematics and orbital periods. The results are discussed in Section 7.

2 OBSERVATIONS AND DATA REDUCTION

The sample of star was selected from Lu (1991) and Jorissen et al. (1998), and the corresponding Ba intensities were taken from there. One normal giant in a Ba-like binary system, HD 66216, was further taken from Jorissen et al. (1998) (originally from the catalogue compiled by Boffin et al. 1993) to check whether this star also has an abnormal Ba abundance based on the high quality spectral data. The basic data on the sample of stars are given in Table 1.

The spectroscopic observations were carried out with the Coudé Echelle Spectrograph equipped with a 1024×1024 TeKtronix CCD attached to the 2.16 m telescope at National Astronomical Observatories, Chinese Academy of Sciences (Xinglong station, China). The red arm of the spectrograph with a 31.6 grooves/mm grating was used in combination with a prism as cross-disperser, providing a good separation between the Echelle orders. With a 0.5 mm slit (1.1"), the resolving power is of the order of $R \sim 30000$ in the camera system at the middle focus. The total wavelength coverage was $5500 \sim 9000 \text{ \AA}$ over 36 orders, and most of the spectra have an S/N ratio greater than 60.

We used the standard ECHELLE package in the MIDAS environment for data reduction and equivalent widths (EW s) measurements of lines. The procedure is: order identification, background subtraction, flat-field correction, order extraction, wavelength calibration, radial velocity shift correction, and continuum normalization. Bias, dark current and scattered-light corrections are included in the background subtraction. The pixel-to-pixel sensitivity variations were corrected by using the flat-field. The wavelength calibration was based on thorium-argon lamp spectra. The EW measurements of spectral lines were done by applying two different methods: direct integration of the line profile and Gaussian fitting. The latter is preferable in the case of weak lines, but unsuitable for strong lines in which the damping wings contribute significantly to the EW . The final EW s are weighted averages of these two measurements, depending on the line intensity (see Zhao et al. 2000 for details). We present part of the spectrum of a star in the sample, HD 212320, in Figure 1(a).

3 ATMOSPHERIC PARAMETERS

The stellar atmospheric model is specified by four parameters: effective temperature, surface gravity, metallicity and microturbulent velocity. For more accurate atmospheric parameters, we perform extinction correction on the observed magnitudes of these stars.

3.1 Extinction

The effective temperature of the stars are determined from photometric indices. Since most of our stars are close to the Galactic plane ($|b| < 30 \text{ deg}$), careful attention must be paid to the reddening corrections. Firstly we calculate the reddening values $E(B - V)$ based on the dust maps of Schlegel et al. (1998). Then we revise the $E(B - V)$ by using the formula presented in Beers et al. (2002, their Eq.(1)) since the Schlegel et al. map may overestimate the reddening values when their reported color excess exceeds about 0.15 mag (Arce & Goodman 1999) or 0.1 mag (Beers et al. 2002). Next, we can obtain the extinction magnitudes in different wavelength bands, A_B , A_V , A_K , A_b and A_y , by using the relative extinction table of Schlegel et al. (1998) which is based on the Galactic extinction law of Cardelli et al. (1989) and O'Donnell (1994). Finally, the extinction-corrected colors $(B - V)$, $(V - K)$ and $(b - y)$

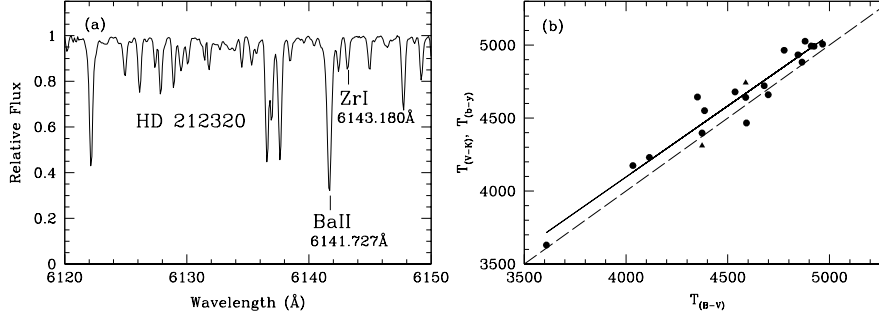


Fig. 1 (a) A part of spectrum of HD 212320 showing Ba II 6141.727 Å, Zr I 6143.180 Å. (b) Comparisons among the three sets of T_{eff} values calculated from $(B - V)$, $(V - K)$ and $(b - y)$ colors for stars in the sample. The filled circles and triangles refer to the temperatures calculated with $(V - K)$ and $(b - y)$, respectively. The solid line is the least-square fit to the points of $T_{\text{eff}}(V - K)$ vs. $T_{\text{eff}}(B - V)$, whereas the dashed diagonal line is the one-to-one relation.

are obtained. The distances D ($=1/\pi$) are estimated from the parallax. All these values are presented in Table 2.

3.2 Effective temperature

Effective temperatures (T_{eff}) are determined from color indices $(B - V)$, $(V - K)$ or $(b - y)$ by using the empirical calibrations of Alonso et al. (1999, 2001) for giant stars. Since the Alonso formula depends on $[\text{Fe}/\text{H}]$, these calculations are done iteratively. Figure 1(b) shows the consistency of the effective temperatures of the sample stars calculated from $(B - V)$, $(V - K)$ and $(b - y)$. The solid line is the least-square fitting (with a slope of 0.97) of $T_{\text{eff}}(V - K)$ vs. $T_{\text{eff}}(B - V)$, and the dashed diagonal line is the one-to-one relation.

Alonso et al. (1999) showed that the effective temperatures determined from $(b - y)$ are more accurate than those from $(B - V)$. Unfortunately, only two stars with $(b - y)$ index are available in our samples. For calculating abundances, we use the effective temperature derived from $(B - V)$ rather than $(V - K)$ since the K magnitude of many samples here are brighter than 4 mag, and these K -band indices often have larger uncertainties. Furthermore, half of the errors for the K magnitude here are higher than 0.2 mag, and a 0.2 mag error in the K band causes an error of about 250 K in effective temperature (for details see Liu et al. 2007). We should keep in mind that the color $(B - V)$ is affected by the CN and C_2 , making the stars redder, and as a result, the temperature derived from this color should be lower (Allen & Barbuy 2006a). Considering the uncertainties in spectral data, in $[\text{Fe}/\text{H}]$, and the errors in the calibration of color-temperature, we estimate that the uncertainty in the effective temperature is about 200 K.

3.3 Surface gravity

There are two methods used to determine the gravity ($\log g$). One is requiring the Fe I and Fe II lines to give the same iron abundance. But it is well known that the derivation of iron abundance from Fe I and Fe II lines may be affected by many factors such as unreliable oscillator strengths, non-local thermodynamic equilibrium (non-LTE) effects and uncertainties in the temperature structure of the model atmospheres. The other method is using the parallaxes measured by the Hipparcos satellite. This method is more precise for bright stars with Hipparcos parallaxes that are as good as the stars studied here. In

this method the following relations are used:

$$\log \frac{g}{g_{\odot}} = \log \frac{M}{M_{\odot}} + 4 \log \frac{T_{\text{eff}}}{T_{\text{eff},\odot}} + 0.4(M_{\text{bol}} - M_{\text{bol},\odot})$$

and

$$M_{\text{bol}} = V + 5 + 5 \log \pi + BC,$$

where M is the stellar mass, M_{bol} the absolute bolometric magnitude, V the visual magnitude, BC the bolometric correction, and π the parallax. We adopt solar value $\log g_{\odot} = 4.44$, $T_{\text{eff},\odot} = 5770$ K, and $M_{\text{bol},\odot} = 4.75$ mag. The parallax (π) and its errors are taken from observations made by the Hipparcos satellite (ESA 1997). Stellar mass was determined from the position of the star in the $M_{\text{bol}} - \log T_{\text{eff}}$ diagram. We adopt the stellar evolution tracks given by Girardi et al. (2000). The bolometric correction, BC , is determined using the empirical calibration of Alonso et al. (1999).

3.4 Metallicities and microturbulent velocity

The initial metallicities of the sample stars were taken from the literature if available. Otherwise, we guessed an initial value by judging from the spectra and the color indices. The final model and chemical composition were derived iteratively. Microturbulent velocity (ξ_t) was determined from the abundance analysis by requiring a zero slope of zero in the relation $[\text{Fe}/\text{H}]$ vs. EWs. The derived atmospheric parameters of the sample stars are summarized in Table 3 including star name, effective temperatures calculated from $(V - K)$, $(b - y)$ and $(B - V)$, metallicity, surface gravity and microturbulent velocity. We checked the atmospheric parameters to make sure that the values we obtained are reliable. As an example in Figure 2 we show for HD 66216 that the abundance deduced from the Fe I lines is independent of the excitation potential (test of effective temperature T_{eff} , Fig. 2a), independent of the EWs of the lines (test of the microturbulent velocity ξ_t , Fig. 2b) and independent of the wavelength (Fig. 2c). In Figure 2(b) it can also be seen that the iron abundance deduced from Fe I lines is the same as the abundance deduced from the Fe II lines (test of gravity $\log g$).

As a comparison, we have six stars in common with McWilliam (1990). He observed 671 giants but in a narrow spectral range (6500 - 6850 Å) and obtained the atmospheric parameters and elemental abundances. In Table 3 we also list the atmospheric parameters of the stars also studied by McWilliam (1990) in the last four columns. The median differences between ours and theirs are $\Delta T_{\text{eff}} = 48$ K, $\Delta \log g = -0.54$, $\Delta [\text{Fe}/\text{H}] = 0.14$ and $\Delta \xi_t = -0.75$.

4 MODEL ATMOSPHERES AND SPECTRAL LINES

We carried out a classical LTE abundance analysis based on a set of plane parallel, line blanketed, flux constant model atmospheres (Kurucz 1993). Abundances are determined by using the atmospheric parameters given in Table 3 (T_{eff} , $(B - V)$, $\log g$, $[\text{Fe}/\text{H}]$ and ξ_t) and the EWs of the lines. For Fe we selected the lines with $20 < \text{EW} < 120$ mÅ, and $20 < \text{EW} < 200$ mÅ for the other elements, because the weaker lines would increase random errors (and possibly some systematic overestimates), while the stronger lines are very sensitive to the microturbulent velocity and the damping. Great care was taken to insure consistency of the continuum level.

In Figure 2(c), as an example, it can be seen that for HD 66216 the abundance deduced from the Fe I lines does not depend on wavelength. The line list of Liu et al. (2009, their table 2) and Liang et al. (2003, their table 3) has been adopted with their excitation potential χ and oscillator strengths $\log gf$.

As mentioned in Liu et al. (2009), the oscillator strengths $\log gf$ of the spectral lines are taken from the NIST database (<http://physics.nist.gov>), Lambert & Warner (1968), Weise & Martin (1980), Biémont et al. (1981, 1982), Hannaford et al. (1982), Fuhr et al. (1988), Luck & Bond (1991), O'Brian et al. (1991), Bard & Kock (1994), Lambert et al. (1996), Nissen & Schuster (1997), Chen et al. (2000), Liang et al. (2003) and the references therein. The $\log gf$ values of the O I 7771-7774 triplet lines and of the neutron capture (n -capture) process elements were taken from Liang et al. (2003, their table 3).

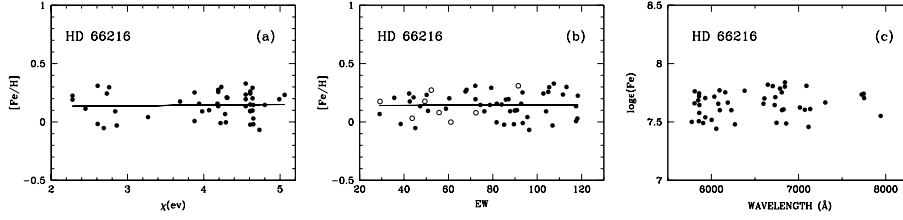


Fig. 2 We check the atmospheric parameters T_{eff} , $\log g$ and ξ_t of the stars by taking HD 66216 as an example: **(a)** There is no significant trend of $[\text{Fe}/\text{H}]$ vs. χ (Fe I line) and the excitation equilibrium suggests that the effective temperature we adopt is reliable. **(b)** The Fe abundances from Fe I lines and Fe II lines are consistent within 0.2 dex, which illustrates the ionization equilibrium. It suggests that the $\log g$ is reliable. It also shows that there is no trend between Fe abundances and EWs of the lines. This means that the ξ_t is reliable. The filled and open circles refer to Fe I and Fe II abundances respectively. The solid lines are the least square fits of the data points. **(c)** It shows no trend from the correlations of Fe abundances (Fe I) with wavelengths, and also indicates the correctly chosen continuum levels.

5 CHEMICAL ABUNDANCES

5.1 The abundance and their uncertainties

The abundances of 17 elements (O, Na, Mg, Al, Si, Ca, Sc, Ti, V, Cr, Mn, Ni, Y, Zr, Ba, La, Eu) in our 19 stars are given in Table 4. The solar abundances are taken from Grevesse & Sauval (1998). Uncertainties in the abundances mainly come from the systematic errors introduced by uncertainties in the atmospheric parameters and the stochastic error arising from random errors in the oscillator strengths, the damping constants and in the measurements of EWs. We ignore the uncertainties in atomic data.

In Table 5 and 6 we computed the variation of $[\text{Fe}/\text{H}]$ and $[\text{X}/\text{Fe}]$ (where X is one of the 17 elements considered here) for a change of 200 K in the effective temperature, 0.2 dex in the surface gravity and 0.2 km/s in the micro turbulence velocity, for two typical stars in our sample, HD 66216 and HD 212320. We expect that the uncertainties in the EW measurements are about ± 5 mÅ. The resulting error in the abundances depends on the EW of the line and has been computed line by line. For an element represented by N lines, the final error on the abundances is divided by a factor \sqrt{N} . The total uncertainty is estimated with the *Least Squares Method* (LSM) and given in Table 5 and 6.

We should keep in mind that since we are using the red spectra for abundance analysis, we only have limited spectral lines of the n -capture process elements to use. For example, only one line of Y I (6435.000 Å) is used, but the Y II lines can result in higher abundances than the Y I line (Gratton & Sneden 1994; Yushchenko et al. 2004). There are four lines of Zr I used to derive Zr abundances, but Zr II line can result in higher abundances than Zr I line (Allen & Barbuy 2006a; Gratton & Sneden 1994; Yushchenko et al. 2004). There are three lines of Ba II (5853.688, 6141.727 and 6496.908 Å) used to derive Ba abundances and two lines of La II (6390.480 and 6774.330 Å) used to derive La abundances. The line of Eu II at 6645.110 Å is used to derive Eu abundances for our sample stars.

5.1.1 $[\text{X}/\text{Fe}]$ vs. the Atomic number Z

Table 4 presents the abundances $\log \epsilon(X)$ (in the usual scale $\log X(\text{H})=12.0$) and the corresponding $[\text{X}/\text{Fe}]$ values for our sample of Ba stars. The two full tables will be published online. In Figure 3 we have plotted $[\text{X}/\text{Fe}]$ vs. the atomic number Z for the 19 stars of our sample. The abundance pattern of the elements from O to Ni is similar to the solar abundance pattern ($[\text{X}/\text{Fe}]$ close to zero although with some scatter), but the n -capture elements Y, Zr, Ba, La, Eu are overabundant relative to the Sun and the

overabundances are different in strong and mild Ba stars. As commented in Lu (1991), the Ba intensity class was estimated visually according to Warner’s procedure (Warner 1965) on a scale of 1 (weakest) to 5 (strongest). Lu (1991, sect. 4.1) called Ba stars with a Ba intensity between 2 and 5 “strong”, and Ba stars with a Ba intensity between 0.3 and 1.5 “weak”. More recently, Jorissen et al. (1998), called Ba stars with a Ba intensity ≤ 2 “mild”, and Ba stars with a Ba intensity of 3, 4 or 5 “strong”.

In this work, we could roughly divided the sample stars as strong Ba stars with Ba intensity Ba=2-5 and mild (weak) Ba stars with Ba<2. However, we will consider [Ba/Fe] abundance ratios as a stricter diagnostic for strong or mild Ba stars. The Ba intensities of the 19 stars in our sample are given in Table 1(second column). It shows that there are six stars with Ba=2-5 (HD 18418, HD 49641, HD 58368, HD 90127, HD 95153, HD 218356). The Ba intensity of HD 224276 is not given by Lu (1991) but we identify it as a strong Ba star since its heavy elements show a pattern similar to HD 95193 and HD 218356 (which are both strong Ba stars with Ba=2.0 m), and its [Ba/Fe] is up to 0.78, which is much higher than the solar value. Thus we suggest its Ba intensity could be assumed to be 2.0. For HD 212320 and HD 58121, although their Ba intensities are 1.5 and 1.0, but their abundances are up to [Ba/Fe] = 1.11 and 0.73, respectively. Thus we also classify them as “strong Ba stars”. Therefore, to diagnose strong Ba stars, we consider their [Ba/Fe] > 0.60. Then nine of the sample stars are strong Ba stars.

The top nine panels of Figure 3 show the abundance patterns of these nine strong Ba stars in our sample. The *n*-capture elements in these nine strong Ba stars show obvious overabundance relative to those in the Sun. The remaining ten panels of Figure 3 show the abundance patterns of ten mild Ba stars in our sample. Among them, the “Ba-like” star HD 66216 has a pattern similar to the mild Ba stars HD 11353 with Ba intensity of 0.1 and HD 31308 with Ba intensity of 0.2. Thus we classify this Ba-like star as a “mild Ba star” and assume its Ba intensity is 0.2. These three stars have [Ba/Fe] of 0.34, 0.36 and 0.32, respectively.

Figure 3 shows that:

–In the strong Ba stars, the first peak *s*-process elements Y and Zr are overabundant (unlike the α - and iron peak elements). The second peak *s*-process elements Ba and La, and the *r*-process element Eu are more overabundant than the first peak ones.

–In the mild Ba stars the first peak elements are not overabundant, and have the same behavior as the α - and iron-peak elements. The second peak of *s*-process elements (Ba and La) is higher than the first peak elements, but is less overabundant than that in the strong Ba stars.

Y and Zr belong to the first peak of the *s*-process (corresponding to the neutron magic number 50), and the core He and shell C burning in massive stars mainly produce these elements (Raiteri et al. 1991a, 1991b, 1992, 1993; Qian & Wasserburg. 2007). Ba, La and Eu belong to the second peak. Ba and La (corresponding to the neutron magic number 82) are mainly generated during shell He burning in AGB stars (Busso et al. 2001), whereas the element Eu is dominantly produced through *r*-process during a supernova explosion (Snedden et al. 2008). As mentioned in Busso et al. (2001, their Sect.2.1), those nuclei whose locations correspond to neutron magic numbers ($N = 50$ and 82) are mainly of *s*-process origin, and act as bottlenecks for the *s*-process path because of their low *n*-capture cross sections. Consequently, for relatively low *s*-process efficiencies, the neutron flux mainly feeds the nuclei at the 1st peak, while for higher exposures, the second peak species are favored.

The overabundances of *n*-capture process elements are lower in mild Ba stars than in strong Ba stars, which could be explained by the relatively weaker neutron exposure in their AGB-companion stars. Stronger neutron exposure will benefit stronger *s*-process nucleosynthesis and lead to higher *s*-process element abundances. If the neutron exposure is not strong enough, the first peak of Y and Zr could show weak overabundance and probably sometimes be close to the solar value. A Ba star having a longer orbital period, meaning there is a larger distance of the two member stars in the binary system, will have less accretion efficiency from its AGB-companion star with *s*-process overabundances. In addition, we only have Y I and Zr I lines to derive Y and Zr abundances in this work. Y I and Zr I will probably result in lower Y and Zr abundances than the Y II line (Gratton & Sneden 1994; Yushchenko et al. 2004) and Zr II line (Allen & Barbuy (2006a, sect.4.7).

5.2 Ba intensity versus [Ba/Fe]

It is interesting to show the relation between [Ba/Fe] and Ba intensity, which is given in Figure 4 for our 19 sample stars (the filled circles) and some Ba stars from Liang et al. (2003, the open circles) and Liu et al. (2009, the open triangles). A linear least-square fit is obtained for these 29 Ba stars as shown by the solid line. This shows a correlation or consistency between Ba intensity and [Ba/Fe] (also see Lu & Uggren 1985), but here we include many objects with lower Ba intensity down to 0.1. Thus our work extends to Ba stars with much weaker overabundances of n -capture process elements, which will be useful for understanding the abundance patterns of Ba stars, from mild to strong Ba cases. The general trend of the increasing [Ba/Fe] following Ba intensity is clearly shown in Figure 4. However, from the [Ba/Fe] value and the abundance patterns, we suggest the two stars HD 212320 and HD 58121 are strong Ba stars with [Ba/Fe] larger than 0.6, although their Ba intensities are 1.5 and 1.0, respectively.

5.2.1 [X/Fe] vs. [Fe/H]

It is interesting to discuss the relation of [X/Fe] vs. [Fe/H] for the 17 elements analyzed in our sample of stars. Our sample stars are distributed in a narrow range of [Fe/H]: $-0.32 < [\text{Fe}/\text{H}] < +0.23$ and thus most of them should be disk stars.

We found that for Na and the iron-peak elements (Sc, Ti, V, Cr, Mn and Ni), [X/Fe] is independent of [Fe/H]. For other elements (Al, α -elements, n -capture elements), [X/Fe] shows slight anti-correlations with [Fe/H].

Figure 5 displays these trends. For n -capture elements, our samples of stars shows increasing [X/Fe] with decreasing [Fe/H]. This anti-correlation is less obvious for Eu. [Ba/Fe] and [La/Fe] show the most overabundant values in our sample stars, up to +1.13 and +1.38, respectively. Eu shows relatively weak overabundances (up to 0.65) since Eu has more contributions from the r -process. However, [Y/Fe] and [Zr/Fe] are not exceptionally overabundant with median values of 0.15 and 0.18, respectively. The ranges of [X/Fe], the median values and the line numbers used in the abundance analyses are given in Table 7 for these 17 elements that were analyzed in our sample stars.

5.2.2 Comparison with the common stars in literature

To compare the abundances of our sample Ba stars with those of the common stars in McWilliam (1990), we compare the $\log \epsilon(X)$ abundances for the six common stars in our work with those of McWilliam (1990) as shown in Figure 6. They indicate that our abundances are generally lower than theirs. The reason could be the result of different atmospheric parameters (Table 3), the different atmospheric models and atomic data, etc. in the two works.

6 KINEMATIC ANALYSIS AND ORBITAL PERIOD

6.1 Kinematic analysis

The kinematic studies of the stars in the solar neighborhood are based on the velocities U , V and W measured along axes pointing respectively towards the Galactic center, the direction of Galactic rotation and the North Galactic Pole. The accurate distances (parallax) and the proper motions available in the Hipparcos Catalogue (ESA 1997), combined with stellar radial velocity, make it possible to derive reliable space velocities. For our sample stars, the proper motion, parallax and radial velocity values are taken from SIMBAD. For some of them without radial velocity measurements, we calculate these radial velocities from the observed spectra and correct them by using the *observatory/astutil/rvcorrect* program in IRAF¹.

¹ IRAF is distributed by the National Optical Astronomical Observatory, which is operated by the Association of Universities for Research in Astronomy, Inc., under cooperative agreement with the National Science Foundation.

The calculation of the space velocity with respect to the Sun is based on the method presented by Johnson & Soderblom (1987). The correction of space velocity to the Local Standard of Rest is based on a solar motion of $(U, V, W)_{\odot} = (10.1, 4.0, 6.7) \text{ km s}^{-1}$ (see Hogg et al. 2005, which is slightly different from the values given in Binney & Merrifield 1998). The mean U , V and W velocities and their distributions are shown in Figure 7.

The mild and strong Ba stars do not present obvious differences in the UV, WV and WU planes (Fig. 7a,b,c), and most of the stars are in the disk. The disk properties of most stars are further confirmed by Figure 7d, their Toomre diagrams $((U^2 + W^2)^{1/2} \text{ vs. } V \text{ velocity})$. There the semi-circular line refers to the limit of thin disk stars, $V_{\text{tot}} = (U^2 + V^2 + W^2)^{1/2} < 85 \text{ km s}^{-1}$ suggested in Chen et al. (2004).

In Lu (1991), the histogram of U , V , W velocities and their distributions in the UV, UW, VW planes (their figs. 8, 9, 10) indicate that the strong Ba stars have a higher velocity dispersion than the weak Ba stars and are, therefore, probably members of the old disk population, whereas the weak Ba stars are members of the young disk population. But in our work, such a difference is not clear, as shown in Figure 7. Maybe the reason is that we have fewer sample stars.

As Jorissen et al. (1998) mentioned, there are several pieces of evidence that mild Ba stars belong to a somewhat younger population than strong Ba stars. Except for the velocity dispersion found in Lu (1991), Mennessier et al. (1997) suggested that mild Ba stars are mostly clump giants with a mass in the range 2.5-4.5 M_{\odot} , whereas strong Ba stars populate the giant branch and have masses in the range 1-3 M_{\odot} . These mass estimates are consistent with those derived from the mass-function distributions in Jorissen et al. (1998) (their fig.9). They also found that although mild Ba stars are dominated by high-mass objects, there is a small tail of less massive objects which suggests that mild Ba stars are indeed a mixture of populations H and L (their fig.11, where H and L mean high and low mass respectively). Some mild Ba stars having low orbital period should be in old population. Metallicity is also a factor that affects the overabundances of s -process elements. Being old objects, they should have rather low mass, but the third dredge-up becomes more efficient for low metallicities (Busso et al. 2001).

6.2 Orbital period

Because Ba stars are binaries, the overabundance of n -capture process elements is due to the transfer of s -enriched material from a previously-AGB-companion star (now a white dwarf) via mass transfer or wind accretion. Thus orbital period is an important parameter that characterizes a Ba star in a binary system. As shown theoretically by figure 4 in Han et al. (1995) and observationally by figure 3 in Začs (2000), strong Ba stars have orbital periods of ~ 1000 days, but the orbital periods of mild Ba stars are longer or shorter. Ba stars with long orbital periods arise from wind accretion. The longer the orbital periods are, the lower the accretion efficiency is. Ba stars with short orbital periods are from stable Roche lobe overflow or a common envelope. The shorter the orbital periods are, the earlier during TP-AGB phase the onset of mass transfer occurs.

There are five sample stars in the present work whose information on orbital periods can be obtained from Jorissen et al. (1998): HD 49641, HD 58121, HD 58368 and HD 95193 are classified as strong Ba stars in this work, and their orbital periods are 1768 d, 1214.3 d, 672.7 d and 1653.7 d, respectively. HD 66216 is classified as a mild Ba star in this work, and its orbital period is 2438 d. The orbital periods of these Ba stars are generally consistent with the suggestions of Han et al. (1995) and Začs (2000). We can understand that this longer orbital period of HD 66216 may result in lower accretion efficiency of n -capture process elements from the AGB-companion star through wind accretion or wind exposure (Han et al. 1995), and thus there is less overabundance of n -capture process elements on it compared to the other four strong Ba stars. In addition, Jorissen et al. (1998) presented the compiled observations of orbital periods of some strong Ba stars in their table 2a, of some mild Ba stars in their table 1a. As shown in figures 2 and 4 of Jorissen et al. (1998), the orbital periods of Ba stars are in a wide range from ~ 200 to 11000 days (with one mild Ba star as 80.53 days), but mild Ba stars generally have much higher orbital periods than the strong Ba stars (as shown by the horizontal axes of their figs.11 and 6). Also, the short-period mode ($P < 1500$ d) comprised of nearly-circular systems is lacking among mild Ba stars

(their Sect.10). It is a pity we did not have the orbital periods for the rest of our 14 sample stars in this study. We hope in the future orbital period information about these remaining stars can be obtained.

7 DISCUSSION AND CONCLUSIONS

The chemical compositions of 19 Ba stars were obtained on the basis of high resolution and high S/N ratio Echelle spectra. We carried out a classical LTE analysis of these stars. From their effective temperature, gravity and metallicity, the 19 Ba stars are giants and belong to the Galactic disk.

Among the 19 stars of our sample, six stars have Ba index larger than 2 and are classified as “strong Ba stars”. For these stars we found $[Ba/Fe] > 0.6$. In HD 224276 (which has no known Ba index), we found its $[Ba/Fe] = 0.78$ and its abundance pattern is similar to those of other strong Ba stars (HD 95193, HD 218356). Thus this star is also a strong Ba star and we assume its Ba index as 2.0. The Ba index of HD 212320 is equal to 1.5, but we found that it has $[Ba/Fe] = 1.11$ thus we suggest it should be classified as a strong Ba star. For HD 58121, this star has $[Ba/Fe] = 0.73$. Although its Ba index is 1.0, we assume this star has been misclassified and it should also be a strong Ba star. Finally in our sample there are nine strong Ba stars with $[Ba/Fe] > 0.6$. The other ten stars can be considered to be mild Ba stars with $+0.17 < [Ba/Fe] < +0.54$. In particular the star HD 66216, classified as “Ba-like star”, should be a mild Ba star with $[Ba/Fe] = 0.34$.

The abundance distributions and the abundance scatter are quite consistent with what is observed for other Ba stars (Allen & Barbuy 2006b; Smiljanic et al. 2007). In strong Ba stars, the n -capture process elements are all overabundant, but this overabundance is higher for the second peak elements (about +0.9 dex for $[Ba/Fe]$ and $[La/Fe]$, and +0.5 dex for $[Eu/Fe]$) than for the first peak elements (about 0.3 dex for Y and Zr). In mild Ba stars, $[Y/Fe]$ and $[Zr/Fe]$ are close to zero (not much overabundance of the first peak elements), but the elements of the second peak: Ba, La and Eu are overabundant (about +0.4 dex for $[Ba/Fe]$ and $[La/Fe]$, and +0.3 dex for $[Eu/Fe]$), this overabundance is lower than in the strong Ba stars.

The abundances of the n -capture elements (Y, Zr, Ba and La but not Eu) show a slight anti-correlation with metallicity $[Fe/H]$, which could mean that the lower metallicity benefits the nucleosynthesis of n -capture process elements.

The kinematic parameters (UVW velocities) of stars in the sample confirm that they are disk stars. Contrary to the findings of Lu (1991) and Jorissen et al. (1998), we did not find an obvious significant difference between the velocities of the strong and mild Ba stars. The reason could be that we have fewer stars than them.

The orbital periods are obtained for five of our sample stars, which show that the mild Ba star HD 66216 (2438 d) has longer orbital period than the other four strong Ba stars HD 49641, HD 58121, HD 58368 and HD 95193 (1768, 1214.3, 672.7 and 1653.7 d, respectively). The orbital periods are consistent with Han et al. (1995) and Zacs (2000), and are in the range of Ba stars given by Jorissen et al. (1998). Further work to obtain the orbital periods of the remaining 14 sample stars will be useful to better understand their evolution.

Acknowledgements We thank the referees for an extensive and helpful review containing very relevant scientific suggestions, which greatly improve this paper. We are grateful to Prof. Jianrong Shi, Kefeng Tan, Shu Liu and Wenyuan Cui for helping with data reduction and analysis. Guochao Yang thanks Guohu Zhong, Yi Hu, Pin Lü, Qiang Liu, Yueyang Zhang, He Gao, Dong Gao and Anbing Ren for their helpful advices and encouragements. This work was supported by the Natural Science Foundation of China (NSFC) Foundation under Nos.11273011, U1231119, 10973006, 11003002, 11273026, 10933001, 10973015; and the National Basic Research Program of China (973 Program) Nos.2007CB815404, 2007CB815403, 2007CB815406.

References

Allen, D. M., & Barbuy, B. 2006a, A&A, 454, 895

- Allen, D. M., & Barbuy, B. 2006b, *A&A*, 454, 917
- Alonso, S., Arribas, S., & Martínez-Roger, C. 1999, *A&AS*, 140, 261
- Alonso, S., Arribas, S., & Martínez-Roger, C. 2001, *A&A*, 376, 1039
- Antipova, L. I., Boyarchuk, A. A., Pakhomov, Yu. V., Panchuk, V. E., 2004, *ARep.*, 48, 597
- Arce, H. G., Goodman, A. A., 1999, *ApJ*, 517, 264
- Bard, A., & Kock, M. 1994, *A&A*, 282, 1014
- Beers, T. C., Drilling, J. S. Rossi, S. et al. 2002, *AJ*, 124,931
- Bidelman, W. P., & Keenan, P. C. 1951, *ApJ*, 114, 473
- Biémont, E., Grevesse, N., Hannaford, P., & Lowe, R. M. 1981, *ApJ*, 248, 867
- Biémont, E., Karner, C., Meyer, G., et al. 1982, *A&A*, 107, 166
- Binney, J., & Merrifield, M. 1998, *Galactic Astronomy* (New Jersey: Princeton Univ. Press, Princeton)
- Boyarchuk, A. A., Pakhomov, Yu. V., Antipova, L. I., Boyarchuk, M. E., 2002, *ARep.*, 46, 819
- Boffin, H. M. J., Cerf, N., & Paulus, G., 1993, *A&A*, 271, 125
- Burbidge, E. M., Burbidge, G. R., Fowler, W. A., & Hoyle, F. 1957, *RvMP*, 29, 547
- Busso, M., Gallino, R., Wasserburg, G. J., 1999, *ARA&A*, 37, 239
- Busso, M., Lambert, D. L., Beglio, L., et al. 1995, *APJ*, 446, 775
- Busso, M., Lambert, D. L., Beglio, L., Travaglio, C., & Smith, V. V. 2001, *APJ*, 557, 802
- Cardelli, J. A., Clayton, G. C., & Mathis, J. S. 1989, *ApJ*, 345, 245
- Carquillat, J. M., Jorissen, A., Udry,S., & Ginestet, N. 1998, *A&AS*, 131, 49
- Chen, Y. Q., Nissen, P. E., Zhao, G., Zhang, H. W., & Benoni, T. 2000, *A&AS*, 141, 491
- Chen, Y. Q., Nissen, P. E., Zhao, G. 2004, *A&A*, 425, 697
- Cowan, J. J., Thielemann, F. K., & Truran, J. W. 1991, *Phys. Rep.*, 208, 267
- ESA 1997, the Hipparcos and Tycho Catalogues, ESA SP-1200
- Fuhr, J. R., Martin, G. A., & Wiese, W. L. 1988, *JPRCD*, 17, Suppl.4
- Gallino, R., Arlandini, C., Busso, M. et al. 1998, *ApJ*, 497, 388
- Girardi, L., Bressan, A., Bertelli, G., & Chiosi, C. 2000, *A&AS*, 141, 371
- Gratton, R. G. & Sneden, C. 1994, *A&A*, 287, 927
- Grevesse, N., & Sauval, A. J. 1998, *Space Sci. Rev.*, 85, 161
- Han, Z. W., Eggleton, P. P., Podsiadlowski, P., & Tout, C. A. 1995, *MNRAS*, 277, 1443
- Hannaford, P., Lowe, R. M., Grevesse, N., Biemont, E., & Whaling, W. 1982, *ApJ*, 261, 736
- Hogg, D. W., Blanton, M. R., Roweis, S. T., Johnston, K. V. 2005, *ApJ*, 629, 268
- Johnson, D. R. H., & Soderblom, D. R. 1987, *AJ*, 93, 864
- Jorissen, A., Van Eck S., Mayor, M., & Udry, S. 1998, *A&A*, 332, 877
- Kovacs, N., 1985, *A&A*, 150, 232
- Kurucz, R. L. 1993, CD-ROM, Vol. 13, Smithsonian Astrophysics Observatory, Cambridge
- Lambert, D. L. 1985, *ASSL*, 114, 191L
- Lambert, D. L. 1988, *IAUS*, 132, 563L
- Lambert, D. L., & Warner, B. 1968, *MNRAS*, 139, 115
- Lambert, D. L., Health, J. H., Lemke, M. et al. 1996, *ApJS*, 103, 183
- Liang, Y. C., Zhao, G., & Zhang, B. 2000, *A&A*, 363, 555
- Liang, Y. C., Zhao, G., Chen, Y. Q., Qiu, H. M., & Zhang, B. 2003, *A&A*, 397, 257
- Liu, G. Q., Liang, Y. C., & Deng, L. C. *RAA* 2009, 4, 431
- Liu, Y. J., Zhao, G., Shi, J. R., et al. 2007, *MNRAS*, 382,553
- Luck, R. E., & Bond, H. E. 1991, *ApJS*, 77, 515
- Lu, P. K., Dawson, D. W., Upgren, A. R., & Weis, E. W. 1983, *ApJS*, 52,169

- Lu, P. K., & Upgren, A. R. 1985, in *Cool Stars with Excess of Heavy Elements*, edited by M. Jасhek and P. C. Keenan (Reidel Dordrecht), P. 25
- Lu, P. K. 1991, *AJ*, 101, 2229
- McClure, R. D. 1984, *PASP*, 96, 117M
- McClure, R. D., Fletcher, J. M., & Nemec, J. M. 1980, *ApJ*, 238, L35
- McWilliam, A. 1990, *ApJS*, 74, 1075
- Mennessier, M. O., Luri, X., Figueras, F. et al. 1997, *A&A*, 326, 722
- Nissen, P. E. & Schuster, W. J. 1997, *A&A*, 326, 751
- O’Brian, T. R., Wickliffe, M. E., Lawler, J. E. et al. 1991, *JOSAB*, 8, 1185
- O’Donnell, J. E. 1994, *ApJ*, 422, 1580
- Pilachowski, C. A., 1977, *A&A*, 54, 465
- Qian, Y. Z. & Wasserburg, G. J. 2007, *PhyRep*, 442,237
- Raiteri, C. M., Busso, M. et al. 1991a, *ApJ*, 367,228
- Raiteri, C. M., Busso, M. et al. 1991b, *ApJ*, 371,665
- Raiteri, C. M., Gallino, R. et al. 1992, *ApJ*, 387,263
- Raiteri, C. M., Gallino, R. et al. 1993, *ApJ*, 419,207
- Schlegel, D. J., Finkbeiner, D. P. & Davis, M. 1998, *ApJ*, 500, 525
- Smith, V. V., 1984, *A&A*, 132, 326
- Smiljanic, R., Porto de Mello G. F., & da Silva L. 2007, *A&A*, 468, 679
- Snedden, C., Cowan, J. J. et al. 2008, *ARA&A*, 46, 241
- Straniero O., Chieffi A., Limongi M., Busso M., Gallino R., Arlandini C. 1997, *ApJ* 478, 332
- Straniero O., Gallino R., Busso M., Chieffi A., Raiteri C. M., Limongi, M., Salaris, M. 1995, *ApJ* 440, L85
- Udry, S., Jorissen, A., Mayor, M., & Van Eck, S. 1998a, *A&AS*, 131, 25
- Udry, S., Mayor, M., Van Eck S., Jorissen A., Prévot L., Grenier, S., & Lindgren H. 1998b, *A&AS*, 131, 43
- Warner, B., 1965, *MNRAS*, 129, 263
- Weise, W. L., & Martin, G. A. 1980, *NSDRS-NBS*, 68
- Yushchenko, A. V., Gopka, V. F., Kim, C., Liang, Y. C., Musaev, F. A., Galazutdinov, G. A., 2004, *A&A*, 413, 1105
- Začs, L. 1994, *A&A*, 283, 937
- Začs, L. 2000, *IAUS*, 177, 277
- Zhao, G., Qiu, H. M., Chen, Y. Q., & Li, Z. W., 2000, *ApJ*, 126, 461

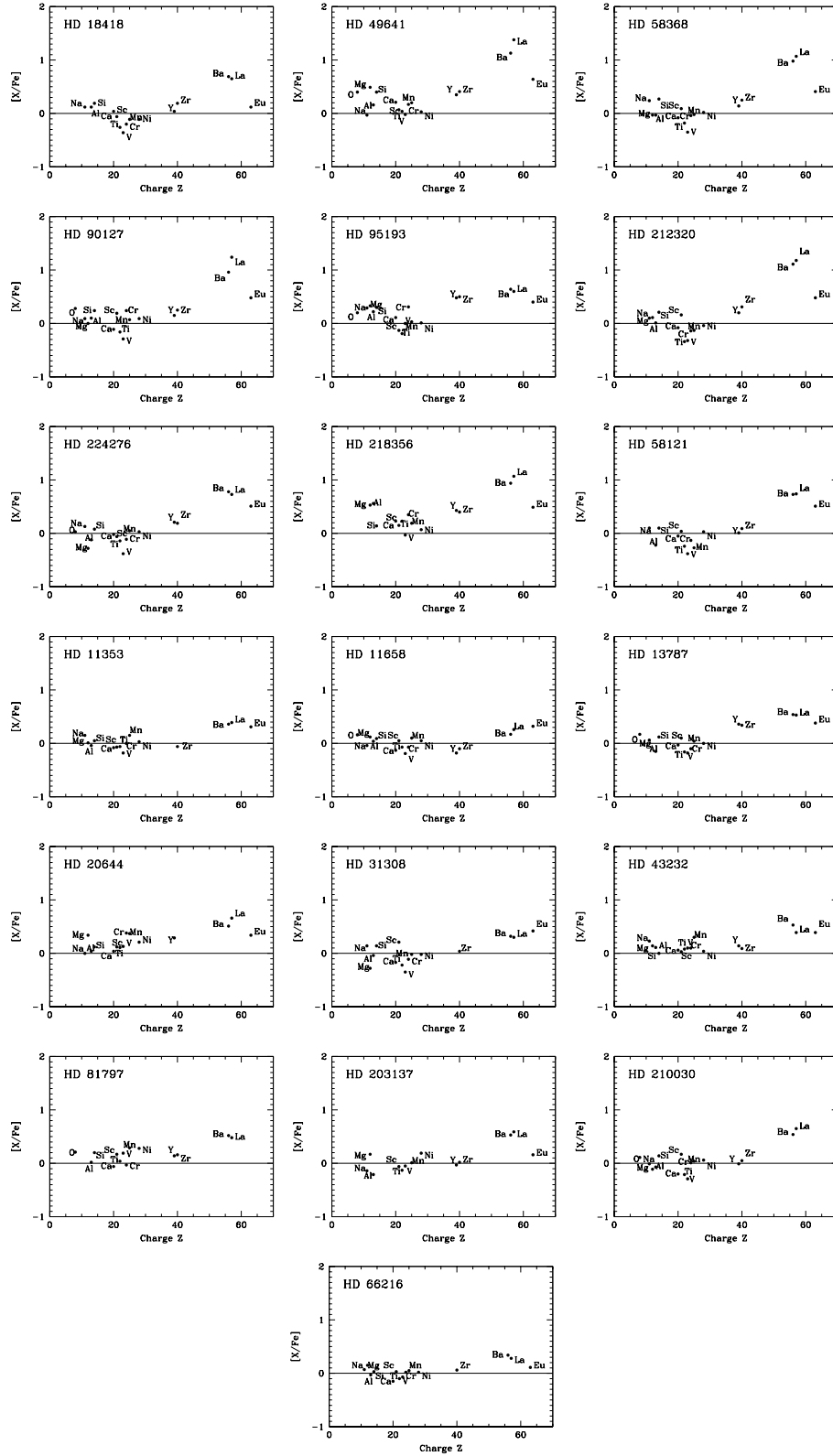


Fig. 3 Abundances of the 19 sample stars: (1) the top nine panels are for the strong Ba stars with $[Ba/Fe] > 0.6$, and the top six among them have Ba intensity $Ba > 2$, but HD 218356 has $Ba = 1.5$ and HD 58121 has $Ba = 1.0$; (2) the remaining ten panels are for the 10 mild Ba stars with Ba intensity of $Ba \leq 1.0$.

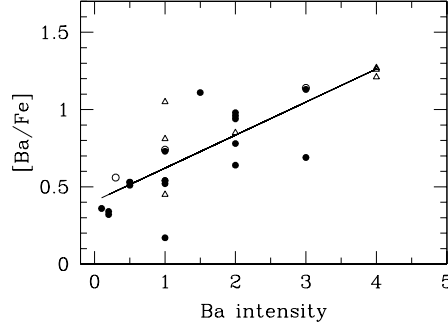


Fig. 4 The $[Ba/Fe]$ vs. Ba intensity relations for the 19 sample stars (the filled circles), and the data points from Liang et al. (2003, the open circles) and Liu et al. (2009, the open triangles). The solid line is linear least-square fit for these data points.

Table 1 Basic Data on the Sample of Stars.

Star name	Ba	Sp.	l	b	ra.	$\delta_{ra.}$	dec.	$\delta_{dec.}$	π (mas)	$\delta\pi$	B	V	K
HD 11353	0.1	K0	165.8823	-68.0481	38.78	0.94	-38.04	0.53	12.59	0.85	4.873	3.738	1.016 [0.250]
HD 11658	1.0c	K0	132.9747	-09.9246	90.98	0.59	-30.35	0.50	4.93	0.84	8.350	7.250	4.675 [0.017]
HD 13787	1.0	K0	140.2071	-20.8720	-19.87	0.81	-7.72	0.69	5.23	1.01	8.250	7.300	5.113 [0.023]
HD 18418	3.0	K0	148.7200	-18.0025	-4.84	1.27	-7.10	0.83	2.99	1.18	8.530	7.540	5.232 [0.020]
HD 20644	0.5	K4	158.1375	-23.4606	-8.21	0.88	-16.42	0.64	5.09	0.90	6.076	4.472	0.877 [0.172]
HD 31308	0.2:	G5	203.9237	-28.4207	8.38	0.95	-2.84	0.69	5.05	1.02	8.340	7.330	5.057 [0.026]
HD 43232	0.5	K1.5	214.4047	-10.9789	-6.18	0.78	-20.06	0.65	5.06	0.90	5.332	3.987	1.087 [0.246]
HD 49641	3.0c	K0	209.4241	+01.2500	-7.08	0.82	-10.46	0.49	0.73	0.88	8.500	7.130	4.253 [0.015]
HD 58121	1.0m	G7	211.1724	+10.1346	0.54	0.89	-0.26	0.57	2.82	0.95	9.090	7.920	5.377 [0.021]
HD 58368	2.0c	K0	210.0191	+11.0233	2.74	0.94	-0.74	0.61	2.36	0.97	8.990	7.970	5.773 [0.023]
HD 66216	bl	K2	193.8981	+27.1407	-28.53	0.83	-35.25	0.64	12.66	0.78	6.087	4.944	— —
HD 81797	1.0:	K3	241.4881	+29.0455	-14.49	0.95	33.25	0.53	18.40	0.78	3.486	2.004	-1.127[0.208]
HD 90127	2.0	K0	249.3141	+42.1085	11.61	1.01	-5.73	0.57	4.55	0.87	8.440	7.270	4.758 [0.027]
HD 95193	2.0m	G8	266.1248	+40.5624	-6.56	1.19	-2.65	0.79	2.30	1.03	9.280	8.300	6.050 [0.021]
HD 203137	0.5	K4.5	092.0166	+00.4142	7.77	0.66	-2.11	0.54	1.91	0.62	8.870	7.000	2.263 [0.278]
HD 210030	1.0	K0	048.8171	-47.8983	9.39	1.07	-27.46	0.56	6.07	0.95	8.570	7.470	5.014 [0.016]
HD 212320	1.5:	G3	055.6592	-49.6862	-6.21	1.19	8.95	0.87	7.10	0.93	6.912	5.922	3.891 [0.270]
HD 218356	2.0m	K0	095.1201	-31.7089	0.26	0.56	-33.31	0.41	6.07	0.67	6.067	4.767	1.765 [0.220]
HD 224276	:	K2	113.0484	-15.8091	6.21	0.70	-0.01	0.62	2.09	0.96	9.48	8.45	6.125 [0.020]

Notes: Ba intensity in column 2. c: certain Ba stars, m: marginal Ba stars, bl: Ba-likely stars, and ":" refers to the case of barium intensity uncertain.

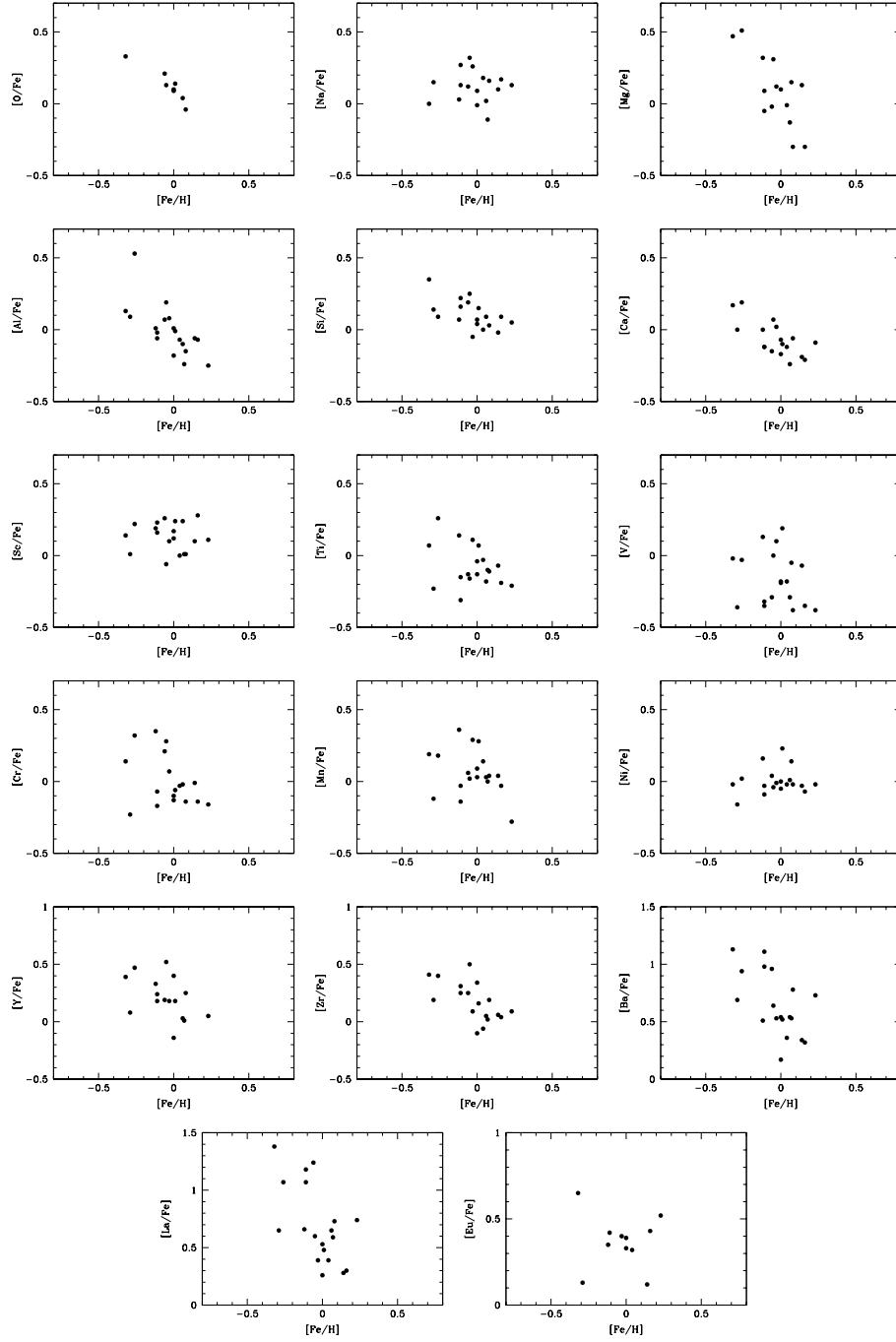


Fig. 5 $[X/Fe]$ vs. $[Fe/H]$ relations for the 19 sample stars, from iron-peak elements to the n -capture elements.

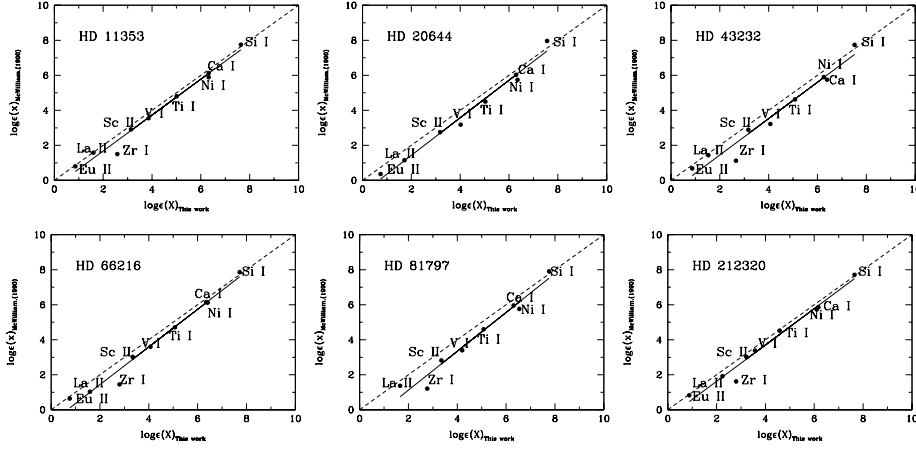


Fig. 6 Comparison of $\log \epsilon(X)$ for ten elements of the six common stars in this work and McWilliam (1990). The solid lines are the least-square fits to the data and the dashed diagonal lines are the one-to-one relation.

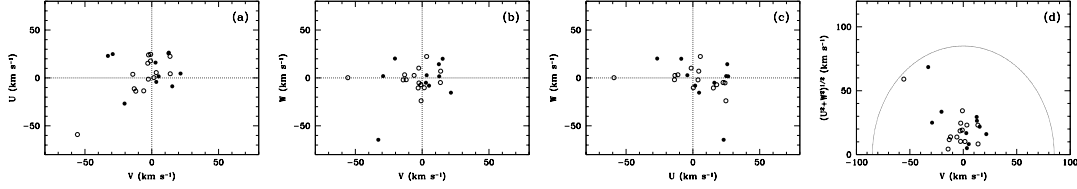


Fig. 7 The U, V and W velocities of our sample stars. The filled circles refer to strong Ba stars (with $Ba \geq 2$) and the open circles refer to mild stars (with $Ba < 2$).

Table 2 The Reddening Values of the Color Indices.

Star name	$(B - V)_o$	$(V - K)_o$	$(b - y)_o$	$E(B - V)$	D (kpc)	A_B	A_V	A_K	A_b	A_y	$(B - V)$	$(V - K)$	$(b - y)$
HD 11353	1.135	2.722	—	0.016	0.079	0.071	0.055	0.006	0.067	0.054	1.119	2.673	—
HD 11658	1.100	2.575	—	0.045	0.203	0.194	0.149	0.017	0.182	0.147	1.055	2.442	—
HD 13787	0.950	2.187	—	0.030	0.191	0.128	0.098	0.011	0.120	0.097	0.920	2.100	—
HD 18418	0.990	2.308	—	0.051	0.334	0.220	0.169	0.019	0.206	0.167	0.939	2.158	—
HD 20644	1.604	3.595	—	0.202 ^a	0.196	0.870	0.668	0.074	0.816	0.660	1.402	3.001	—
HD 31308	1.010	2.273	—	0.017	0.198	0.074	0.057	0.006	0.069	0.056	0.993	2.223	—
HD 43232	1.345	2.900	—	0.114 ^a	0.198	0.491	0.377	0.042	0.460	0.373	1.231	2.565	—
HD 49641	1.370	2.877	—	0.147 ^a	1.370	0.636	0.489	0.054	0.597	0.483	1.223	2.442	—
HD 58121	1.170	2.543	0.667	0.024	0.355	0.103	0.079	0.009	0.097	0.078	1.146	2.473	0.649
HD 58368	1.020	2.197	—	0.021	0.424	0.090	0.069	0.008	0.085	0.069	0.999	2.135	—
HD 66216	1.143	—	—	0.009	0.079	0.040	0.031	0.003	0.038	0.030	1.134	—	—
HD 81797	1.482	3.131	—	0.010	0.054	0.042	0.032	0.004	0.039	0.032	1.472	3.102	—
HD 90127	1.170	2.512	—	0.032	0.220	0.138	0.106	0.012	0.130	0.105	1.138	2.418	—
HD 95193	0.980	2.250	—	0.047	0.435	0.202	0.155	0.017	0.190	0.153	0.933	2.112	—
HD 203137	1.870	4.737	—	0.048	0.524	0.208	0.160	0.018	0.195	0.158	1.822	4.595	—
HD 210030	1.100	2.456	—	0.026	0.165	0.112	0.086	0.009	0.105	0.085	1.074	2.380	—
HD 212320	0.990	2.031	—	0.044	0.141	0.188	0.144	0.016	0.176	0.143	0.946	1.903	—
HD 218356	1.300	3.002	0.835	0.086	0.165	0.372	0.286	0.032	0.349	0.283	1.214	2.748	0.768
HD 224276	1.030	2.325	—	0.071	0.478	0.307	0.236	0.026	0.288	0.233	0.959	2.115	—

Notes: $(B - V)_o$, $(V - K)_o$, $(b - y)_o$ and $(B - V)$, $(V - K)$, $(b - y)$ are the values observed and after extinction correction respectively.

D is obtained directly from the parallaxes ($D = 1/\pi$). The superscript a indicates that these stars are heavily reddened, thus their colors (and temperatures) are uncertain, and the resulting masses and ages may have larger uncertainties.

Table 3 The atmospheric parameters of the sample stars and the comparison of six common stars with that of McWilliam (1990, Mc).

Star name	$T_{\text{eff}}(V - K)$	$T_{\text{eff}}(b - y)$	$T_{\text{eff}}(B - V)$	$\log g$	[Fe/H]	ξ_t (km s ⁻¹)	$T_{\text{eff(Mc)}}$	$\log g_{\text{(Mc)}}$	[Fe/H] _(Mc)	$\xi_{t(\text{Mc})}$
HD 11353	4467	—	4592	2.13	0.04	1.45	4600	2.70	-0.13	2.2
HD 11658	4660	—	4699	2.61	0.00	1.50	—	—	—	—
HD 13787	5007	—	4966	2.90	0.00	1.40	—	—	—	—
HD 18418	4934	—	4845	2.36	-0.29	1.60	—	—	—	—
HD 20644	4231	—	4115	1.18	-0.12	1.60	3980	1.56	-0.31	2.6
HD 31308	4884	—	4865	2.84	0.16	1.60	—	—	—	—
HD 43232	4551	—	4386	1.40	-0.03	1.55	4270	2.22	-0.18	2.6
HD 49641	4645	—	4351	1.05	-0.32	1.50	—	—	—	—
HD 58121	4642	4743	4588	2.41	0.23	1.35	—	—	—	—
HD 58368	4965	—	4777	2.47	-0.11	1.50	—	—	—	—
HD 66216	—	—	4588	2.43	0.14	1.38	4540	2.73	0.03	1.7
HD 81797	4175	—	4034	1.23	0.01	1.50	4120	1.77	-0.12	2.6
HD 90127	4680	—	4536	2.36	-0.06	1.43	—	—	—	—
HD 95193	4992	—	4924	2.62	-0.05	1.57	—	—	—	—
HD 203137	3630	—	3609	0.60	0.07	1.45	—	—	—	—
HD 210030	4722	—	4679	2.73	0.06	1.50	—	—	—	—
HD 212320	5027	—	4880	2.63	-0.11	1.50	4790	2.87	-0.25	2.2
HD 218356	4398	4311	4374	1.54	-0.26	1.45	—	—	—	—
HD 224276	4994	—	4910	2.56	0.08	1.45	—	—	—	—

Table 4 Elemental Abundances of the Sample Stars.

	HD 11353		HD 11658		HD 13787		HD 18418		HD 20644		HD 31308		HD 43232	
el	log $\epsilon(X)$	[X/Fe]	log $\epsilon(X)$	[X/Fe]	log $\epsilon(X)$	[X/Fe]	log $\epsilon(X)$	[X/Fe]	log $\epsilon(X)$	[X/Fe]	log $\epsilon(X)$	[X/Fe]	log $\epsilon(X)$	[X/Fe]
Fe I	7.55	—	7.51	—	7.51	—	7.21	—	7.39	—	7.67	—	7.48	—
Fe II	7.61	—	7.53	—	7.53	—	7.21	—	7.51	—	7.78	—	7.38	—
O I	—	—	8.99	0.16	9.00	0.17	—	—	—	—	—	—	—	—
Na I	6.52	0.15	6.29	−0.04	6.39	0.06	6.16	0.12	6.22	0.00	6.63	0.14	6.53	0.23
Mg I	7.63	0.01	7.70	0.12	—	—	—	—	7.81	0.34	7.46	−0.28	7.69	0.14
Al I	6.47	−0.04	6.51	0.04	6.32	−0.15	6.30	0.12	6.40	0.04	6.59	−0.04	6.55	0.11
Si I	7.64	0.05	7.64	0.09	7.67	0.12	7.45	0.19	7.56	0.12	7.85	0.14	7.52	0.00
Ca I	6.32	−0.08	6.23	−0.13	6.33	−0.03	6.11	0.04	6.29	0.04	6.35	−0.17	6.39	0.06
Sc II	3.14	−0.07	3.22	0.05	3.27	0.10	2.82	−0.06	3.18	0.12	3.54	0.21	3.17	0.03
Ti I	5.01	−0.06	4.96	−0.07	4.87	−0.16	4.48	−0.26	5.03	0.11	4.97	−0.22	5.08	0.08
V I	3.86	−0.18	3.81	−0.19	3.82	−0.18	3.35	−0.36	4.02	0.13	3.81	−0.35	4.07	0.10
Cr I	5.71	0.00	5.60	−0.07	5.57	−0.10	5.18	−0.20	5.94	0.38	5.72	−0.11	5.74	0.10
Mn I	5.58	0.15	5.49	0.10	5.43	0.04	4.99	−0.11	5.65	0.37	5.53	−0.02	5.66	0.30
Ni I	6.32	0.03	6.30	0.05	6.25	0.00	5.85	−0.11	6.35	0.21	6.39	−0.02	6.26	0.04
Y I	—	—	2.06	−0.18	2.60	0.36	1.99	0.04	2.42	0.29	—	—	2.35	0.14
Zr I	2.58	−0.06	2.50	−0.10	2.94	0.34	2.50	0.19	—	—	2.80	0.04	2.66	0.09
Ba II	2.53	0.36	2.30	0.17	2.67	0.54	2.53	0.69	2.53	0.51	2.61	0.32	2.63	0.53
La II	1.60	0.39	1.43	0.26	1.70	0.53	1.53	0.65	1.72	0.66	1.63	0.30	1.53	0.39
Eu II	0.86	0.31	0.83	0.32	0.89	0.38	0.34	0.12	0.74	0.34	1.09	0.42	0.87	0.39

	HD 49641		HD 58121		HD 58368		HD 66216		HD 81797		HD 90127		HD 95193	
el	log $\epsilon(X)$	[X/Fe]	log $\epsilon(X)$	[X/Fe]	log $\epsilon(X)$	[X/Fe]	log $\epsilon(X)$	[X/Fe]	log $\epsilon(X)$	[X/Fe]	log $\epsilon(X)$	[X/Fe]	log $\epsilon(X)$	[X/Fe]
Fe I	7.19	—	7.74	—	7.40	—	7.65	—	7.52	—	7.45	—	7.46	—
Fe II	6.99	—	7.84	—	7.55	—	7.64	—	7.52	—	7.47	—	7.51	—
O I	8.91	0.40	—	—	—	—	—	—	9.05	0.21	9.05	0.28	8.98	0.20
Na I	5.98	−0.03	6.66	0.10	6.46	0.24	6.54	0.07	—	—	6.36	0.09	6.57	0.29
Mg I	7.75	0.49	—	—	7.44	−0.03	7.87	0.15	—	—	7.52	0.00	7.86	0.33
Al I	6.31	0.16	6.48	−0.22	6.33	−0.03	6.58	−0.03	6.50	0.02	6.51	0.10	6.64	0.22
Si I	7.63	0.40	7.88	0.10	7.71	0.27	7.72	0.03	7.76	0.20	7.73	0.24	7.80	0.30
Ca I	6.25	0.21	6.54	−0.05	6.17	−0.08	6.35	−0.15	6.31	−0.06	6.19	−0.11	6.42	0.11
Sc II	2.92	0.07	3.44	0.04	3.15	0.09	3.34	0.03	3.35	0.17	3.30	0.19	2.99	−0.13
Ti I	4.75	0.04	5.02	−0.24	4.74	−0.18	5.07	−0.10	5.08	0.04	4.81	−0.16	4.79	−0.19
V I	3.66	−0.02	3.85	−0.38	3.54	−0.35	4.07	−0.07	4.20	0.19	3.65	−0.29	3.95	0.00
Cr I	5.52	0.17	5.77	−0.13	5.52	−0.04	5.83	0.02	5.65	−0.03	5.85	0.24	5.93	0.31
Mn I	5.27	0.20	5.35	−0.27	5.26	−0.02	5.58	0.05	5.69	0.29	5.40	0.07	5.37	0.03
Ni I	5.96	0.03	6.51	0.03	6.16	0.02	6.41	0.02	6.54	0.28	6.28	0.09	6.21	0.01
Y I	2.27	0.35	2.48	0.01	2.27	0.14	—	—	2.39	0.14	2.33	0.15	2.67	0.48
Zr I	2.69	0.41	2.92	0.09	2.74	0.25	2.80	0.06	2.77	0.16	2.79	0.25	3.05	0.50
Ba II	2.94	1.13	3.09	0.73	3.00	0.98	2.61	0.34	2.66	0.52	3.03	0.96	2.72	0.64
La II	2.23	1.38	2.14	0.74	2.13	1.07	1.59	0.28	1.66	0.48	2.35	1.24	1.72	0.60
Eu II	0.83	0.64	1.25	0.51	0.81	0.41	0.76	0.11	—	—	0.93	0.48	0.86	0.40

	HD 203137		HD 210030		HD 212320		HD 218356		HD 224276	
el	log $\epsilon(X)$	[X/Fe]	log $\epsilon(X)$	[X/Fe]	log $\epsilon(X)$	[X/Fe]	log $\epsilon(X)$	[X/Fe]	log $\epsilon(X)$	[X/Fe]
Fe I	7.58	—	7.57	—	7.40	—	7.25	—	7.59	—
Fe II	7.70	—	7.71	—	7.56	—	7.29	—	7.65	—
O I	—	—	9.00	0.11	—	—	—	—	8.94	0.03
Na I	6.26	−0.14	6.38	−0.01	6.32	0.10	—	—	6.54	0.13
Mg I	7.82	0.17	7.53	−0.11	7.58	0.11	7.87	0.53	7.38	−0.28
Al I	6.33	−0.21	6.46	−0.07	6.37	0.01	6.79	0.56	6.43	−0.12
Si I	—	—	7.75	0.14	7.65	0.21	7.45	0.14	7.71	0.08
Ca I	—	—	6.22	−0.20	6.17	−0.08	6.35	0.23	6.42	−0.02
Sc II	3.18	−0.06	3.40	0.17	3.22	0.16	3.08	0.15	3.19	−0.06
Ti I	4.97	−0.13	4.88	−0.21	4.58	−0.34	5.02	0.23	4.97	−0.14
V I	4.02	−0.05	3.77	−0.29	3.57	−0.32	3.73	−0.03	3.70	−0.38
Cr I	—	—	5.74	0.01	5.42	−0.14	5.78	0.35	5.64	−0.11
Mn I	5.47	0.01	5.49	0.04	5.15	−0.13	5.34	0.19	5.52	0.05
Ni I	6.51	0.19	6.37	0.06	6.10	−0.04	6.08	0.07	6.36	0.03
Y I	2.28	−0.03	2.29	−0.01	2.33	0.20	2.43	0.43	2.53	0.21
Zr I	2.69	0.02	2.71	0.05	2.80	0.31	2.76	0.40	2.87	0.19
Ba II	2.73	0.53	2.73	0.54	3.13	1.11	2.83	0.94	2.99	0.78
La II	1.83	0.59	1.88	0.65	2.24	1.18	2.00	1.07	1.98	0.73
Eu II	0.74	0.16	—	—	0.88	0.48	0.76	0.49	1.10	0.51

Table 5 Uncertainties in the Abundance Analysis for a Sample Star HD 66216.

	σ_{EW}/\sqrt{N}	ΔT_{eff}	$\Delta \log g$	$\Delta[\text{Fe}/\text{H}]$	$\Delta \xi_t$	σ_{total}
		200	0.2	0.15	0.2	LSM
$\Delta[\text{Fe I}/\text{H}]$	0.01	0.02	0.04	0.02	0.04	0.06
$\Delta[\text{Fe II}/\text{H}]$	0.02	0.15	0.01	0.03	0.01	0.15
$\Delta[\text{Na I}/\text{Fe}]$	0.02	0.12	0.05	0.05	0.05	0.15
$\Delta[\text{Mg I}/\text{Fe}]$	0.05	0.02	0.01	0.01	0.01	0.06
$\Delta[\text{Al I}/\text{Fe}]$	0.04	0.08	0.03	0.04	0.03	0.11
$\Delta[\text{Si I}/\text{Fe}]$	0.02	0.12	0.01	0.01	0.02	0.12
$\Delta[\text{Ca I}/\text{Fe}]$	0.01	0.14	0.08	0.08	0.07	0.19
$\Delta[\text{Sc II}/\text{Fe}]$	0.03	0.05	0.03	0.01	0.04	0.08
$\Delta[\text{Ti I}/\text{Fe}]$	0.02	0.13	0.08	0.09	0.08	0.20
$\Delta[\text{V I}/\text{Fe}]$	0.07	0.1	0.11	0.11	0.11	0.23
$\Delta[\text{Cr I}/\text{Fe}]$	0.03	0.12	0.07	0.07	0.07	0.17
$\Delta[\text{Mn I}/\text{Fe}]$	0.02	0.12	0.06	0.04	0.06	0.15
$\Delta[\text{Ni I}/\text{Fe}]$	0.01	0.01	0.05	0.03	0.05	0.08
$\Delta[\text{Y I}/\text{Fe}]$	0.08	0.23	0.01	0.01	0.01	0.24
$\Delta[\text{Zr I}/\text{Fe}]$	0.04	0.22	0.01	0.01	0.01	0.22
$\Delta[\text{Ba II}/\text{Fe}]$	0.02	0.01	0.07	0.01	0.07	0.10
$\Delta[\text{La II}/\text{Fe}]$	0.03	0.04	0.01	0.03	0.01	0.06
$\Delta[\text{Eu II}/\text{Fe}]$	0.07	0.01	0.01	0.04	0.01	0.08

Table 6 Uncertainties in the Abundance Analysis for a Sample Star HD 212320.

	σ_{EW}/\sqrt{N}	ΔT_{eff}	$\Delta \log g$	$\Delta[\text{Fe}/\text{H}]$	$\Delta \xi_t$	σ_{total}
		200	0.2	0.15	0.2	LSM
$\Delta[\text{Fe I}/\text{H}]$	0.01	0.13	0.01	0.01	0.07	0.15
$\Delta[\text{Fe II}/\text{H}]$	0.03	0.15	0.11	0.06	0.06	0.21
$\Delta[\text{O I}/\text{Fe}]$	0.04	0.19	0.06	0.01	0.03	0.21
$\Delta[\text{Na I}/\text{Fe}]$	0.06	0.16	0.01	0.01	0.03	0.17
$\Delta[\text{Mg I}/\text{Fe}]$	0.03	0.06	0.01	0.01	0.02	0.07
$\Delta[\text{Al I}/\text{Fe}]$	0.02	0.11	0.01	0.01	0.02	0.11
$\Delta[\text{Si I}/\text{Fe}]$	0.03	0.02	0.03	0.02	0.04	0.06
$\Delta[\text{Ca I}/\text{Fe}]$	0.02	0.21	0.03	0.02	0.09	0.23
$\Delta[\text{Sc II}/\text{Fe}]$	0.08	0.02	0.08	0.04	0.08	0.15
$\Delta[\text{Ti I}/\text{Fe}]$	0.01	0.17	0.01	0.03	0.07	0.19
$\Delta[\text{V I}/\text{Fe}]$	0.04	0.19	0.01	0.01	0.06	0.20
$\Delta[\text{Cr I}/\text{Fe}]$	0.03	0.18	0.01	0.01	0.06	0.19
$\Delta[\text{Mn I}/\text{Fe}]$	0.03	0.22	0.02	0.01	0.12	0.25
$\Delta[\text{Ni I}/\text{Fe}]$	0.01	0.13	0.02	0.03	0.08	0.15
$\Delta[\text{Y I}/\text{Fe}]$	0.07	0.15	0.04	0.2	0.02	0.26
$\Delta[\text{Zr I}/\text{Fe}]$	0.05	0.2	0.02	0.16	0.02	0.26
$\Delta[\text{Ba II}/\text{Fe}]$	0.02	0.05	0.04	0.07	0.09	0.13
$\Delta[\text{La II}/\text{Fe}]$	0.05	0.05	0.09	0.05	0.1	0.16
$\Delta[\text{Eu II}/\text{Fe}]$	0.09	0.01	0.09	0.05	0.03	0.14

Table 7 The Range of 17 Elements in Our Sample Stars, and the Line Numbers used in the Abundance Analyses.

[X/Fe]	lines	range	median	[X/Fe]	lines	range	median
O I	3	[0.03, 0.40]	0.18	Cr I	7	[−0.20, 0.38]	−0.02
Na I	7	[−0.14, 0.29]	0.10	Mn I	3	[−0.27, 0.37]	0.05
Mg I	9	[−0.28, 0.53]	0.12	[Fe I/H]	60	[−0.32, 0.23]	0.00
Al I	6	[−0.22, 0.56]	0.01	Ni I	44	[−0.11, 0.28]	0.03
Si I	38	[0.00, 0.40]	0.14	Y I	1	[−0.18, 0.48]	0.15
Ca I	27	[−0.20, 0.23]	−0.06	Zr I	4	[−0.10, 0.50]	0.18
Sc II	5	[−0.13, 0.21]	0.07	Ba II	3	[0.17, 1.13]	0.54
Ti I	12	[−0.34, 0.23]	−0.14	La II	2	[0.26, 1.38]	0.65
V I	3	[−0.38, 0.19]	−0.18	Eu II	1	[0.11, 0.64]	0.40